Int. J. Heat Mass Transfer. Vol. 35, No. 1, pp. 187–194, 1992
Printed in Great Britain

0017–9310/92 $5.00 + 0.00

Natural convection in porous media—II. Freezing

H. LEIN and RICHARD S. TANKIN
Department of Mechanical Engineering, Northwestern University, Evanston, IL 60201, U.S.A.

(*Received* 15 *February* 1990 *and in final form* 27 *December* 1990)

Abstract—Freezing and melting experiments are conducted to visualize the interaction between natural convection and the phase change process in porous media. Landau's transformation is applied to solve the irregular moving boundary problem and the computed results agree well with the experimental data. It is found that the natural convection process is controlled by the mean Rayleigh number and weakens as the freezing process proceeds. Various aspect ratios are examined and they agree reasonably well with Beck's preferred formula for a rectangular box.

INTRODUCTION

THE PROBLEM investigated in this paper is phase change in a porous medium. This study is an extension of an earlier study of phase change (freezing) in a non-porous medium [1]. Dietsche and Müller [2] studied the interactions between the solidification process and Bénard convection for a single component fluid experimentally. They found that when the solidification layer is thick compared to the liquid layer, a hysteresis loop exists for liquid layer heights in the range of subcritical Rayleigh numbers. They also observed bimodal patterns characterized by two different length scales when the Rayleigh number is above the critical value. The influence of lateral walls on the interfacial pattern was also included in their paper, i.e. polygonal and roll pattern selection. Chellaiah and Viskanta [3] investigated the freezing of water in a saturated porous medium in the presence of natural convection. They studied the vertical heating case with isothermal boundaries on the sides. When the wall superheat is sufficiently high to induce natural convection, the interface becomes nonplanar and local freezing rates vary. They mentioned the need for flow visualization, especially a non-intrusive method; and an efficient numerical method to improve the simulation of the freezing process. Numerical and analytical methods have been developed for a non-porous medium dealing with a freezing front (moving boundary problem). The analytical methods include the heat balance integral method, the perturbation method and the series expansion method. Several numerical methods are available [4] for handling freezing in a non-porous environment; for example, the Murray–Landis method, the variable time step method, the enthalpy formulation method and Landau's transformation method. For the Murray–Landis method, one has to assume the initial position of the interface and the initial temperature distribution of the solid phase. It is noted that the choice of the initial position has a considerable effect on the required solution time. The variable time step method determines the time step such that the interface traverses one space mesh during that time. Special attention is needed to determine the proper time steps when the movement of the interface is very slow. The enthalpy formulation method transforms the temperature variable to the enthalpy variable. It eliminates the conditions to be specified at the interface and thus it is easy to model the mushy zone between both phases. In some special cases, this formulation will result in some non-physical temperature plateau profiles. In this study, Landau's transformation method will be adopted to solve the moving boundary solidification problem in a porous medium. The basic idea is as follows: the solid–liquid interface is immobilized by introducing a new non-dimensional variable which expresses the location of a point within the phase (both the frozen phase and the non-frozen phase) as the ratio of its distance from the interface and the instantaneous thickness of the phase (for both the frozen phase and the non-frozen phase). With this transform, the original curvilinear non-uniform grids (as seen in Fig. 1) will be transformed into two regular uniform grids which are ideal for numerical calculations. This method has been applied to one-dimensional freezing problems by Beaubouff and Chapman [5]; and to two-dimensional freezing problems by Saith [6] and Sparrow *et al.* [7]. Gadgil and Gobin [8] applied this method to investigate a two-dimensional melting process for pure liquid within a rectangular enclosure in the presence of natural convection. This transformation has two advantages. (1) It is easy to apply to solid–liquid interface problems that have a complicated shape and surface boundaries. (2) There are no difficulties encountered when adding the effects of natural convection within the liquid. However, when this method is applied to two-dimensional problems, it generally results in complex equations that require iterative methods to obtain a solution.

MATHEMATICAL FORMULATION

Within the rectangular domain, natural convection and freezing processes proceed simultaneously. We

NOMENCLATURE

A aspect ratio, L/H
$C(X, t)$ height of the non-frozen phase at X and t
$F(X, Y, t)$ function of the interface
g gravitational constant [m s^{-2}]
H height of the test section [m]
H_s, L_f latent heat of fusion [J kg^{-1}]
K permeability [m^2]
k_s, k_l thermal conductivity [W m^{-1} °C^{-1}]
L width of the test section [m]
n unit vector at interface
$\ddot{q}_s$, $\ddot{q}_l$ heat flux at interface
Ra Rayleigh number, $Kg\beta\Delta TH/v\alpha$
t time [s]
S normalization factor, $C(X, t)/L$
T, T_m, ΔT temperature [°C]
X horizontal Cartesian coordinate
Y, ΔY_l, ΔY_s vertical Cartesian coordinate.

Greek symbols
α thermal diffusivity [m^2 s^{-1}]
β thermal expansion coefficient
v kinematic viscosity [m s^{-2}]
ρ density [kg m^{-3}]
ψ stream function.

Subscripts
C cold plate
crit onset of instability
H hot plate
l non-frozen phase
m interface
n out normal direction
s frozen phase.

consider the quasi steady state condition and assume the freezing front velocity is much less than the liquid motion velocity. This assumption is valid after the initial freezing front establishes itself. Initially for freezing to occur, it was necessary to cool the top plate below the freezing temperature (subcooled). Thus when freezing occurs, the freezing front rapidly extends into the test section as far as the freezing isotherm. This initial freezing phenomenon, which occurs in less than 1 min, is not included in this analysis. By assuming quasi steady state, the computation of the flow field in the non-frozen phase is steady state for each time step. Figure 2 is the domain of this two-phase system, for which we have the following system of equations:

non-frozen phase

$$\frac{\partial^2\psi}{\partial X^2} + \frac{\partial^2\psi}{\partial Y^2} = -\frac{Kg\beta}{v}\frac{\partial T_l}{\partial X} \tag{1a}$$

$$\frac{\partial^2 T_l}{\partial X^2} + \frac{\partial^2 T_l}{\partial Y^2} = \frac{1}{\alpha}\left(\frac{\partial\psi}{\partial Y}\frac{\partial T_l}{\partial X} - \frac{\partial\psi}{\partial X}\frac{\partial T_l}{\partial Y}\right) \tag{1b}$$

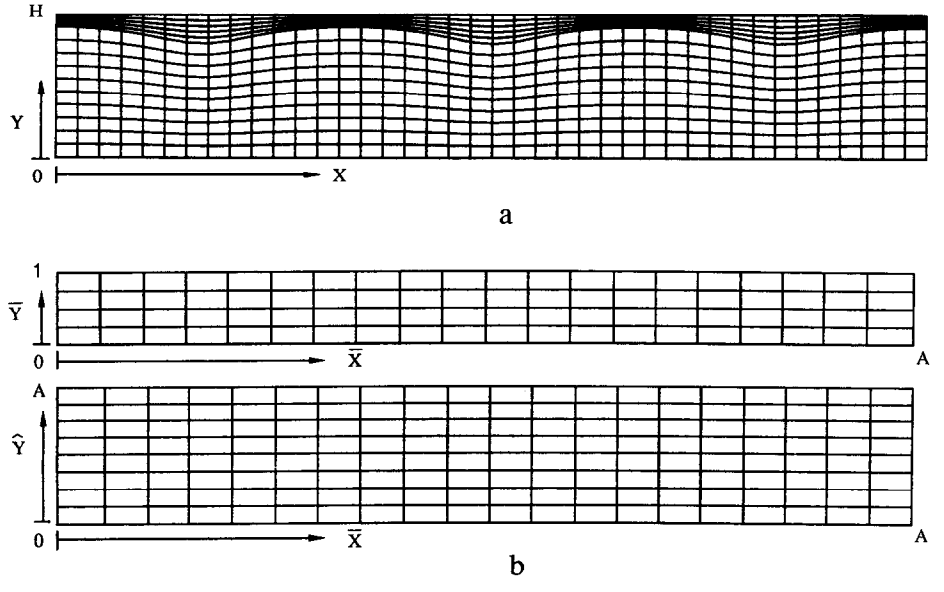

FIG. 1. Schematic diagram of the Landau transformation: (a) physical grid; (b) computation grid where the frozen (upper) and non-frozen (lower) phases are shown.

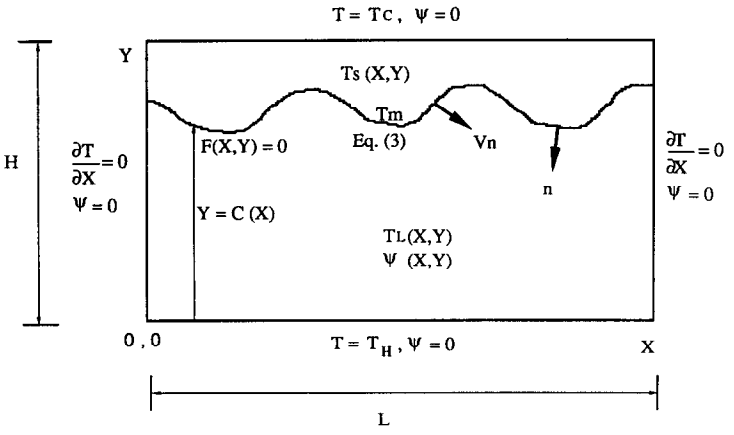

FIG. 2. Boundary conditions applied to the freezing of a porous medium.

frozen phase

$$\frac{\partial^2 T_s}{\partial X^2}+\frac{\partial^2 T_s}{\partial Y^2}=0 \tag{2}$$

interface condition

$$k_s\frac{\partial T_s}{\partial n}-k_l\frac{\partial T_l}{\partial n}=\rho H_s V_n \quad \text{at} \quad F(X,Y,t)=0 \tag{3}$$

where $F(X, Y, t) = 0$ is the interface position and H_s the latent heat of liquid in the porous medium. V_n is the freezing front velocity directed into the liquid phase and k_s, k_l are thermal conductivities of the solid and liquid phase, respectively. The boundary conditions for such a system are:

non-frozen phase

$$\begin{aligned}\psi=0,\quad T_l=T_m \quad &\text{at} \quad F(X,Y,t)=0\\ \psi=0,\quad T_l=T_H \quad &\text{at} \quad Y=0\\ \psi=0,\quad \frac{\partial T_l}{\partial X}=0 \quad &\text{at} \quad X=0,L\end{aligned} \tag{4}$$

frozen phase

$$\begin{aligned}\psi&=0\\ T_s=T_m \quad &\text{at} \quad F(X,Y,t)=0\\ T_s=T_c \quad &\text{at} \quad Y=H\\ \frac{\partial T_s}{\partial X}=0 \quad &\text{at} \quad X=0,L.\end{aligned} \tag{5}$$

Equation (3) is not suitable for numerical discretization because the interface is not flat under natural convection. A two-dimensional rectangular coordinate expression of equation (3) is needed for computation. After manipulation [9], equation (3) becomes

$$\left[1+\left(\frac{\partial C}{\partial X}\right)^2\right]\left[k_s\frac{\partial T_s}{\partial Y}-k_l\frac{\partial T_l}{\partial Y}\right]=\rho H_s\frac{\partial C}{\partial t} \quad \text{at} \quad Y=C(X,t). \tag{6}$$

Equation (6) is in a form ideal for numerical discretization. Equation (3) or equation (6) is basically an energy balance at the interface.

Another difficulty occurs with the boundary conditions as shown in equations (4) and (5). Since it is a moving boundary problem, the interface position is not only a function of X and Y but also of time. In order to overcome this difficulty, we adopted a coordinate transform (Landau's transform, as described previously) to alleviate this problem. By introducing the following new variables, the computational domain becomes regular and uniform:

non-frozen phase

$$\hat{\psi}=\frac{\psi}{\alpha},\quad \hat{T}_l=\frac{T_l-T_C}{T_H-T_C}$$

$$\hat{X}=\frac{X}{H},\quad \hat{Y}=\frac{Y}{HS},\quad S=\frac{C(X,t)}{L} \tag{7}$$

frozen phase

$$\hat{T}_s=\frac{T_s-T_C}{T_H-T_C}$$

$$\hat{X}=\frac{X}{H},\quad \hat{Y}=\frac{Y-C(X,t)}{H-C(X,t)}=\frac{Y/L-S}{1/A-S}$$

$$S=\frac{C(X,t)}{L},\quad A=\frac{L}{H}. \tag{8}$$

Substituting these non-dimensionalizing variables into equations (1) and (2) yields:

non-frozen phase

$$\frac{\partial^2\hat{\psi}}{\partial\hat{X}^2}+\frac{1}{S^2}\frac{\partial^2\hat{\psi}}{\partial\hat{Y}^2}=\frac{-Kg\beta\Delta TH}{\nu\alpha}\frac{\partial\hat{T}_l}{\partial\hat{X}}=-Ra\frac{\partial\hat{T}_l}{\partial\hat{X}}$$

$$\frac{\partial^2\hat{T}_l}{\partial\hat{X}^2}+\frac{1}{S^2}\frac{\partial^2\hat{T}_l}{\partial\hat{Y}^2}=\frac{1}{S}\left(\frac{\partial\hat{\psi}}{\partial\hat{Y}}\frac{\partial\hat{T}_l}{\partial\hat{X}}-\frac{\partial\hat{\psi}}{\partial\hat{X}}\frac{\partial\hat{T}_l}{\partial\hat{Y}}\right) \tag{9}$$

with the following boundary conditions:

$$\frac{\partial \hat{T}_l}{\partial \hat{X}} = 0, \quad \hat{\psi} = 0 \quad \text{at} \quad \hat{X} = 0, A$$

$$\hat{T}_l = 1, \quad \hat{\psi} = 0 \quad \text{at} \quad \hat{Y} = 0$$

$$\hat{T}_l = \frac{T_s - T_C}{T_H - T_C}, \quad \hat{\psi} = 0 \quad \text{at} \quad \hat{Y} = A \qquad (10)$$

frozen phase

$$\frac{\partial^2 \hat{T}_s}{\partial \hat{X}^2} + \frac{1}{(1-AS)^2} \frac{\partial^2 \hat{T}_s}{\partial \hat{Y}^2} = 0 \qquad (11)$$

with the following boundary conditions:

$$\frac{\partial \hat{T}_s}{\partial \hat{X}} = 0 \quad \text{at} \quad \hat{X} = 0, A$$

$$\hat{T}_s = 0 \quad \text{at} \quad \hat{Y} = 1$$

$$\hat{T}_s = \frac{T_s - T_C}{T_H - T_C} \quad \text{at} \quad \hat{Y} = 0. \qquad (12)$$

The interface equation remains unchanged. For steady state computation, the position of the interface can be obtained by setting the time derivative term in equation (6) equal to zero. Thus yielding

$$k_s \frac{\partial T_s}{\partial Y} = k_l \frac{\partial T_l}{\partial Y}$$

$$\Rightarrow k_s \frac{1}{(H-LS)} \frac{\partial^2 T_s}{\partial \hat{Y}} = \frac{k_l}{HS} \frac{\partial \hat{T}_l}{\partial \hat{Y}}$$

$$\Rightarrow C(X) = \frac{k_l L \dfrac{\partial \hat{T}_l}{\partial \hat{Y}}}{k_s \dfrac{\partial \hat{T}_s}{\partial \hat{Y}} + k_l A \dfrac{\partial \hat{T}_l}{\partial \hat{Y}}}. \qquad (13)$$

The finite difference method is employed to discretize the coupled differential equations. The same procedures described in Part I [10] are used to compute the flow and the temperature field of the non-frozen phase; in the frozen phase, the pure conduction calculation is involved. Equation (13) is solved after the temperature profiles in both phases are obtained. The newly obtained solution $C(X)$ is used as a tentative boundary to compute the flow field of the non-frozen phase and the temperature field of the frozen phase. Iteration continues until the flow field and the temperature field in both phases, as well as the interface position, converge to a final value, corresponding to each experimental condition. As for the grid points, 41 were chosen for the horizontal direction in both phases, 41 for the vertical direction in the non-frozen phase and 31 for the frozen phase.

FREEZING EXPERIMENTS

Since the experimental setup is essentially the same as described in Part I, only differences in the setup will be described here. A slightly different size test section was used—36.83 cm wide, 6.1 cm high and 5.61 cm deep. In these tests it was necessary to reduce the top plate temperature to below 0°C (below the lower limit of our circulating bath) in order for freezing to occur. To achieve these low temperatures, thermal electric devices were attached to the top plate. Thermal electric devices were also attached to the bottom plate, providing fine control of the bottom plate temperature. A schematic diagram of the device is shown in Fig. 3. The complex structure of these cooling (or heating) thermoelectric devices might cause non-uniformity of surface temperatures. To alleviate this possibility the following design was adopted. There is a 0.63 cm (0.25 in.) clearance between the thermoelectric devices, and between the thermoelectric devices and the edge of the plates. The thermoelectric devices are soldered to a brass plate that is 1.23 cm (0.5 in.) thick. To further ensure that the temperature is uniform, a 1.23 cm thick stainless steel (304) plate is attached to the brass plate with a layer of thermal conducting compound between them. The temperature variation over the surface of the plate in contact with the porous medium (stainless steel) is less than 0.1°C. The size of the thermoelectric devices (3.96×3.96 cm) determines the width of the plates (5 cm). Since the devices are wired in series, their number (which determines the length of the plates) was limited by the d.c. power supplies available.

As we have seen, the isotherms are visible in the non-frozen phase; however, this is not the case for the frozen phase. The frozen layer consists of solid ethyl salicylate and glass beads whose indices of refraction do not match. Thus, the frozen layer is opaque and the freezing front it easily observed. Again the entire temperature field of the non-freezing phase can be visualized using an incandescent light source.

It was necessary to determine, for the numerical calculations, the thermal conductivity of the solidified porous medium. A pure conduction experiment was set up to determine this quantity. The bottom plate was maintained at room temperature and the top plate was cooled to its lowest value—the limit of the thermal electric devices—thus establishing a thick frozen layer. The Rayleigh number based on the distance and temperature difference between the bottom plate and the solid–liquid interface was not sufficient to induce convection in the non-frozen phase. The solid–liquid interface was flat—having no undulations. After about 3 h steady state conditions had been fully achieved. During this experiment, the isotherms in the non-frozen phase were monitored using the dye laser. These isotherms were straight and did not change their positions when steady state was achieved. For pure conduction with no internal heat sources, the heat transfer across the solid–liquid interface is continuous. Thus

$$\ddot{q}_s \text{ at interface} = \ddot{q}_l \text{ at interface}$$

$$\Rightarrow k_s = k_l \frac{T_H - T_m}{T_m - T_C} \frac{\Delta Y_s}{\Delta Y_l} \qquad (14)$$

where k_s is the thermal conductivity of frozen porous medium, k_l the thermal conductivity of non-frozen porous medium, ΔY_l the distance from the bottom plate to the interface, ΔY_s the distance from the top

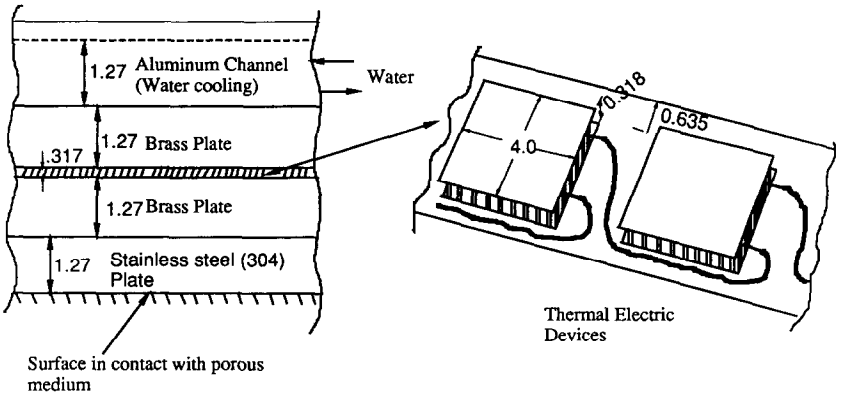

FIG. 3. Schematic diagram showing the structure of the cooling and heating plates (all dimensions are in cm).

plate to the interface, and T_m the melting temperature (interface temperature). In this manner, the thermal conductivity of the solidified porous medium is found to be 0.408 W m^{-1} °C^{-1} (for the non-solidified porous medium $k_1 = 0.528$ W m^{-1} °C^{-1}). Another important thermal property needed is the latent heat of the porous medium during the freezing (or melting) process. Accordingly, the following empirical formula (*Chemical Engineers' Handbook* [11]) was used:

$$13.5 = \frac{L_f \text{ (cal g-mol}^{-1}\text{ K}^{-1})}{T_f \text{ (K)}}$$

$$\Rightarrow L_f = 19.25 \text{ (cal g}^{-1}) = 93\,671 \text{ (J kg}^{-1}) \quad (15)$$

where L_f is the latent heat and T_f the freezing temperature.

Since the interface, during the freezing experiment is not flat when convection is present, a mean value of the height (distance between the bottom plate and the interface) is used in defining a mean Rayleigh number. This mean Rayleigh number is represented as $(\overline{Ra})$.

A typical freezing experiment was performed as follows: a convection pattern was established by raising the bottom plate temperature to 50.6°C and lowering the top plate temperature to 5.9°C (well above the equilibrium freezing temperature of ethyl salicylate). The data were determined using the laser light source and are shown as discrete points in Fig. 4. After sufficient time (several hours), a steady state condition is reached (see Fig. 4(a)). The top plate temperature is constantly monitored with a strip chart recorder. The mixture must be subcooled before freezing will occur. By adjusting the power to the thermal electric devices, the temperature of the top plate is reduced to −6.8°C and maintained at this subcooled temperature (freezing temperature is 2.5°C) until freezing begins. When freezing begins, the top plate temperature suddenly rises, then begins its return to −6.8°C. This sudden rise in the plate temperature is due to the latent heat of freezing. The initial freezing period (when the temperature rises), lasts about 40–50 s. The solid–liquid interface has undulations that match the isotherm pattern in the non-frozen phase. After steady state has been reached, the pattern in Fig. 4(b) is observed. These data were taken about 2 h after the top plate temperature returned to −6.8°C. The height of the nonfrozen porous layer has been reduced. The temperatures of the interface (2.5°C) and the bottom plate (50.6°C) are fixed. This reduction in height accounts for the reduction of $\overline{Ra}$ and the corresponding reduction in the intensity of the rolls. The top plate temperature was then decreased suddenly (by dialing in the appropriate power to the thermal electric devices) to −10.8°C; after steady state was reached (in 2–3 h), the results are shown in Fig. 4(c). The intensity of the rolls have further decreased and the liquid–solid interface has become flatter (matching the isotherm pattern). Figure 4(d) shows the steady state pattern when the top plate temperature is −13.6°C. The convection has further weakened; the mean Rayleigh number is 42.5 which is slightly larger than the critical Rayleigh number. This process was repeated until the top plate temperature reached −16.7°C (the limit of the thermal electric devices). The convection was so weak at this stage (Fig. 4(e)) that the heat transfer mode in the porous medium was almost pure conduction. The mean Rayleigh number associated with this condition is 40.8, which is slightly above the critical Rayleigh number of 39.5.

After the freezing experiments were completed, melting experiments were conducted. The top plate temperature was increased from −16.7 to −13.8°C (Fig. 4(f)). As the temperature of the top plate was increased, the convection cells began to grow as the freezing front retreated. Steady state was achieved within 2 h. When the top plate temperature was further increased (−10.8°C), tiny bubbles appeared at the interface (Fig. 4(g)). These bubbles are believed to be from the dissolved air in the ethyl salicylate that is released during freezing, and accumulates at the solid–liquid interface as the freezing front retreats. This has a twofold effect: (1) it interferes with the observation of the interface, and (2) it affects the heat transfer. As the top plate temperature further

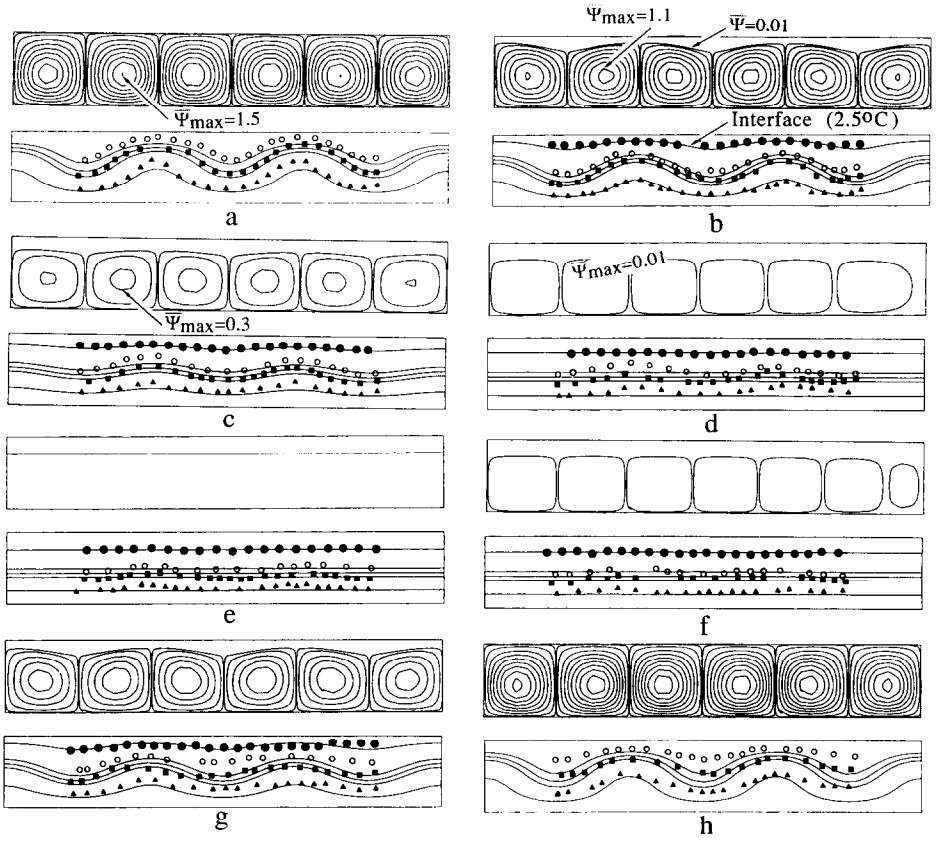

FIG. 4. Plots comparing the numerical and experimental results: (a) $\overline{Ra} = 50.5$; (b) $\overline{Ra} = 47.3$; (c) $\overline{Ra} = 44.3$; (d) $\overline{Ra} = 42.4$; (e) $\overline{Ra} = 40.8$; (f) $\overline{Ra} = 42$; (g) $\overline{Ra} = 45.7$; (h) $\overline{Ra} = 51.9$. The theoretical isotherms (solid lines) are as follows: 2.5, 18.6, 24.1, 26 and 38.2°C. The experimental isotherms—2.5, 18.6, 26 and 38.2°C are represented by ●, ○, ■ and ▲ respectively. Streamlines are also shown.

increases, this phenomenon (appearance of bubbles) became more significant (Fig. 4(h)); resulting in a melting–freezing process that is irreversible. The temperature field is different than the corresponding pattern that appeared during freezing stages. When the temperature of the top plate was brought back to 4.9°C, all the frozen zone had melted (Fig. 4(i)). In an effort to eliminate these bubbles, the ethyl salicylate was boiled before mixing it with glass beads. The results, however, were pretty much the same—maybe fewer bubbles were released. Unfortunately, air may have been re-absorbed by the ethyl salicylate during the filling (and mixing) process. During the melting stage the experimentally determined isotherm patterns are not as regular as those in the freezing stage due to the existence of bubbles which accumulate at the frozen interface.

The effect of the aspect ratio of the test section on the number of cells in the test section was examined. By setting the top plate temperature equal to −15.3°C and the bottom plate temperature equal to 43.2°C, the frozen layer extends into the test section resulting in $\overline{Ra} = 34.4$ ($< Ra_{crit}$). The reduced depth of the non-frozen porous medium resulted in an increase of the aspect ratio of the test section from 6.0 to 8.1. The bottom plate is then heated so that $\overline{Ra} = 43.7$ ($> Ra_{crit}$), and the number of cells present in the test section is eight. Then the temperature of the bottom plate was incrementally increased resulting in an incremental melting of the frozen layer (and also an increase in Rayleigh number). In this manner the aspect ratio of the test section was incrementally changed from 8.1 to 6.0 (when the frozen layer is completely melted). Although the aspect ratio of the test section changes, the number of rolls (eight) in the test section does not change. Thus, the cell size depends on the initial geometry and does not change after the rolls develop—even though the aspect ratio of the test section changes from 8.1 to 6.0.

Beck [12] used both a linear stability analysis and an energy method to obtain a formula for the preferred mode (which is the change between m rolls to $m+1$ rolls) based on the aspect ratio of the test section. In these experiments (Parts I and II) the aspect ratio was varied in several ways: (1) by increasing the test section width—keeping the height fixed; (2) by decreasing the height of the test section—keeping the width fixed; and (3) by freezing—which in effect decreases the height of the test section, while maintaining the 'top plate' temperature constant

Table 1. Aspect ratio of test section and number of rolls in test section

Dimension width × height × depth	Aspect ratio of test section, h_l	$h_{l,min}$ $m-1 \rightarrow m$	$h_{l,max}$ $m \rightarrow m+1$	Roll number predicted by Beck [12] (m)	Roll number measured in experiment
Test section I 54.60 × 7.54 × 4.78 cm	7.24	6.48	7.48	7	8
Test section II 36.83 × 6.10 × 5.61 cm	6.04	5.48	6.48	6	6
Test section II with freezing 36.83 × 4.56 × 5.61 cm	8.08	7.48	8.49	8	8
Test section II with reduced height 36.83 × 2.95 × 5.61 cm	12.50	12.49	13.49	13	12

(2.5°C). Table 1 shows a comparison between the measured roll number and the roll number predicted by Beck. The agreement is reasonably good.

NUMERICAL SIMULATIONS

The steady state numerical simulation starts with established rolls in the porous medium and no freezing—just as the experiments were performed; say, $\overline{Ra} = 50.5$ (see Fig. 4(a)). The temperature field (solid lines) obtained numerically are superimposed on the experimental data in Fig. 4. The temperature of the top plate is reduced to a subcooled temperature −6.8°C when freezing commences (see Fig. 4(b)); the resulting $\overline{Ra} = 47.3$. The streamline $\bar{\psi} = 0.01$ corresponds to the $T = 2.5$°C isotherm, which is the freezing front. As the freezing front moves down, convection is suppressed, and the undulations of the isotherms (solid lines in figures) become weaker. The streamline plot shows the rolls are distorted, as if squeezed by the interface. The freezing front does not shift the rolls in a horizontal direction; the rolls are distorted but the wavelength of the cells (λ) remain the same. Before freezing the maximum stream function ($\bar{\psi}_{max}$) is 1.5 (see Fig. 4(a)); after freezing $\bar{\psi}_{max} = 1.1$ (see Fig. 4(b))—indicating a decrease in the strength of convection. The top plate temperature in the numerical simulation was then set at −10.8°C which corresponds to $\overline{Ra} = 44.3$ (Fig. 4(c)). The flow and temperature field for $\overline{Ra} = 47.3$ were used as initial guess and iterated until the convergence criterion of 10^{-5} was met. Again the streamline $\bar{\psi} = 0.01$ ($T = 2.5$°C) represents the freezing front—which moves further down and further suppresses the convection. The maximum stream function is 0.3. For the case $\overline{Ra} = 42.4$ (Fig. 4(d)) and 40.8 (Fig. 4(e)), the isotherms become flat and the maximum stream function in Fig. 4(d) is 0.01. That is, there is essentially no convection present—heat transfer is by conduction. In Fig. 4(d), the streamline plots show an asymmetry in the horizontal direction due to a relaxation of the convergence criterion to 10^{-4} instead of 10^{-5}. Since the convergence rate depends on the flow field and temperature field, it is very slow when the flow is nearly zero. The agreement is generally good between experiments and the numerical results.

The computations to simulate the melting process are the reverse of the freezing process (see Figs. 4(f)–(h)). As the boundary temperature increases, the interface retreats and the convection rolls become more intense and the undulations of the isotherms increase. Likewise the interface (2.5°C isotherm) becomes wavy. The generation of bubbles in the experiments during the melting process (Figs. 4(e)–(h)) causes discrepancies between experiments and numerical calculations.

From the temperature field, the Nusselt number distribution is computed at each freezing state. Table 2 shows the average Nusselt number vs $\overline{Ra}$. As $\overline{Ra}$ decreases the strength of natural convection decreases. When $\overline{Ra} = 40.86$, which is close to the critical Rayleigh number, the Nusselt number is almost unity;

Table 2. Average Nusselt number along bottom plate and interface during freezing–melting process

Freezing stage			Melting stage		
Mean Rayleigh number	Average Nusselt number at bottom	Average Nusselt number at interface	Mean Rayleigh number	Average Nusselt number at bottom	Average Nusselt number at interface
50.5	1.215	1.203	40.8	1.000	1.000
47.3	1.119	1.126	42.0	1.000	1.000
44.3	1.011	1.012	43.7	1.002	1.003
42.4	1.000	1.000	45.7	1.066	1.070
40.8	1.000	1.000	51.9	1.248	1.232

that is, conduction heat transfer completely dominates. Also from Table 2 it is seen that the average Nusselt number at the bottom plate and interface agree within 1%. This further substantiates the convergence of the numerically computed flow field. The local Nusselt number distributions along the interface and bottom plate are out of phase; similar to the results which were obtained in the non-freezing studies (Part I). Also the local Nusselt number distributions along the bottom plate for various $\overline{Ra}$ are similar to those obtained in Part I.

CONCLUSIONS

The freezing and melting experiments were conducted on a porous medium, and isotherm visualizations were presented. The use of the Landau transformation in the numerical simulations yielded results that agree with experiments for steady state conditions. The natural convection process is controlled by the mean Rayleigh number (as expected) and weakens as the freezing process proceeds. The effects of various aspect ratios were examined and they agree reasonably well with Beck's preferred mode formula for a rectangular box.

Acknowledgements—The authors wish to thank the National Science Foundation for support of this study. This study was supported under grant number MEA8405128.

REFERENCES

1. R. Farhadieh and R. S. Tankin, A study of the freezing of sea water, *J. Fluid Mech.* **71**(2), 293 (1975).
2. C. Dietsche and U. Müller, Influence of Bénard convection on solid–liquid interfaces, *J. Fluid Mech.* **164,** 249 (1985).
3. S. Chellaiah and R. Viskanta, Freezing of water-saturated porous media in the presence of natural convection: experiments and analysis, *J. Heat Transfer* **111,** 425 (1989).
4. T. C. Chawly, *Annual Review of Numerical Fluid Flow.* Hemisphere, Washington, DC (1980).
5. R. T. Beaubouff and A. J. Chapman, Freezing of fluid in forced flow, *Int. J. Heat Mass Transfer* **10,** 1581 (1967).
6. T. Saith, Numerical methods for multidimensional freezing problems in arbitrary domain, *Int. J. Heat Mass Transfer* **100,** 294 (1978).
7. E. M. Sparrow, S. Ramadhyani and S. V. Patankar, Effect of subcooling on cylindrical melting, *Trans. ASME, J. Heat Transfer* **100,** 395 (1978).
8. A. Gadgil and D. Gobin, Analysis of two dimensional melting in rectangular enclosure in presence of convection, *J. Heat Transfer* **106,** 21 (1984).
9. M. N. Ozisik, *Heat Conduction*, p. 403. Wiley, New York (1980).
10. H. Lein and R. S. Tankin, Natural convection in porous media—I. Nonfreezing, *Int. J. Heat Mass Transfer* **35,** 175–186 (1992).
11. R. H. Perry and C. H. Chilton, *Chemical Engineers' Handbook*, 5th Edn, pp. 3–239. McGraw-Hill, New York (1973).
12. J. L. Beck, Convection in a box of porous material saturated with fluid, *Physics Fluids* **15**(8), 1377 (1972).

CONVECTION NATURELLE DANS LES MILIEUX POREUX—II. CONGELATION

Résumé—On réalise des expériences de congélation et de fusion pour visualiser l'interaction entre la convection naturelle et le mécanisme de changement de phase dans les milieux poreux. La transformation de LANDAU est appliquée pour résoudre le problème de frontière mobile irrégulière et les résultats du calcul s'accordent bien avec les données expérimentales. On trouve que le mécanisme de convection naturelle est contrôlé par le nombre de RAYLEIGH moyen et s'affaiblit quand apparait le mécanisme de congélation. Différents rapports de forme sont examinés et ils s'accordent raisonnablement bien avec la formule de BECK pour une cavité rectangulaire.

NATÜRLICHE KONVEKTION IN PORÖSEN MEDIEN—II. MIT GEFRIERVORGANG

Zusammenfassung—Um die Wechselwirkung zwischen natürlicher Konvektion und den Vorgängen der Phasenänderung in porösen Medien sichtbar zu machen, werden Gefrier- und Schmelzversuche durchgeführt. Das Problem der ungleichmäßig bewegten Grenzen wird mit Hilfe der Transformation von Landau gelöst. Die Rechenergebnisse stimmen gut mit Versuchsdaten überein. Es zeigt sich, daß der Vorgang der natürlichen Konvektion von der mittleren Rayleigh-Zahl gesteuert wird und mit dem Fortschreiten des Gefriervorgangs schwächer wird. Es werden unterschiedliche Abmessungsverhältnisse untersucht, wobei sich eine verhältnismäßig gute Übereinstimmung mit der von Beck vorgeschlagenen Formel für den rechteckigen Hohlraum ergibt.

ЕСТЕСТВЕННАЯ КОНВЕКЦИЯ В ПОРИСТЫХ СРЕДАХ—II. ЗАМОРАЖИВАНИЕ

Аннотация—Проведены эксперименты по замораживанию и оттаиванию с целью визуализации взаимодействия между процессами естественной конвекции и фазового перехода в пористых средах. Задача движущейся границы неправильной формы решается с использованием преобразования Ландау. Получено хорошее согласие Между результатами расчета и экспериментальными данными. Найдено, что процесс естественной конвекции определяется средним числом Рэлея и ослабевает по мере развития процесса замораживания. Рассматриваются различные отношения сторон, и обнаружено, что они удовлеворительно описываются уравнением Бека для объема прямоугольной формы.